

Frequency and mode change in the large deflection and post-buckling of compact and thin-walled beams

Original

Frequency and mode change in the large deflection and post-buckling of compact and thin-walled beams / Pagani, A.; Augello, R.; Carrera, E.. - In: JOURNAL OF SOUND AND VIBRATION. - ISSN 0022-460X. - STAMPA. - 432:(2018), pp. 88-104. [10.1016/j.jsv.2018.06.024]

Availability:

This version is available at: 11583/2709916 since: 2018-08-23T16:56:46Z

Publisher:

Elsevier

Published

DOI:10.1016/j.jsv.2018.06.024

Terms of use:

openAccess

This article is made available under terms and conditions as specified in the corresponding bibliographic description in the repository

Publisher copyright

Elsevier postprint/Author's Accepted Manuscript

© 2018. This manuscript version is made available under the CC-BY-NC-ND 4.0 license
<http://creativecommons.org/licenses/by-nc-nd/4.0/>. The final authenticated version is available online at:
<http://dx.doi.org/10.1016/j.jsv.2018.06.024>

(Article begins on next page)

Frequency and mode change in the large deflection and post-buckling of compact and thin-walled beams

A. Pagani,* R. Augello,† E. Carrera‡

*Mul*² Group

Department of Mechanical and Aerospace Engineering, Politecnico di Torino
Corso Duca degli Abruzzi 24, 10129 Torino, Italy.

Abstract: *This paper deals with the investigation of normal modes change of metallic structures, when subjected to geometrical nonlinearities in the large displacement/rotations field. Namely, a unified framework based on the Carrera Unified Formulation (CUF) and a total Lagrangian approach are employed to formulate higher order beam theories including geometric nonlinearities. Thus, a finite element approximation is used along with a path-following method to perform nonlinear analyses. Linearized vibration modes around equilibrium states and along the whole equilibrium path of structures subjected to bending and compression loadings are evaluated by solving a linear eigenvalue problem. In order to show the capabilities of the proposed methodology, both solid and thin-walled cross-section beams are considered. The analyses demonstrate that, with some differences depending on the geometry and both boundary and loading conditions, natural frequencies and modal shapes may change ruinously as the structure is subjected to large displacements and rotations.*

Keywords: Carrera unified formulation; Geometrical nonlinearities; Nonlinear vibrations; Mode aberration.

1 Introduction

Determination of natural frequencies and associated mode shapes play a crucial role in structural verification and analysis. Inherently, external loading and service condition may significantly cause large displacements and rotations, which eventually lead to considerable pre-stress states within the structure. As a consequence, because the modal behavior of structures are evidently a property of the equilibrium state, natural frequencies are subjected to changes. In this regard, Biot [1] provided a nonlinear theory of elasticity and showed the effects that high initial stress has on the equilibrium and vibrations; similarly Herrmann [2] and Odgen and Roxburgh [3] investigated the pre-stress influence on the vibration and stability of elastic and viscoelastic plates. Similar approaches can be found in real applications and in the recent literature, see Abramovich *et al.* [4] and Lurie [5]. These authors introduced a non-destructive

*Assistant Professor. Corresponding author. E-mail: alfonso.pagani@polito.it

†PhD Student. E-mail: riccardo.augello@polito.it

‡Professor of Aerospace Structures and Aeroelasticity

methodology for measuring the buckling condition. Essentially, the stability loads were determined by interpolating, until singularity, the natural frequency of the structure subjected to progressive higher loadings.

Regardless of nonlinear effects, vibrations of structures have been widely studied from scientists and researchers. Leissa [6, 7, 8] described classical plate and shell theories for various shapes and material. Many other authors applied the free vibration method to their study to evaluate dynamic properties of structures, with different loading and boundary cases. As an example, Tseng and Dugundji [9] analyzed nonlinear vibration of a buckled beam, while Yamaki [10, 11] investigated clamped beams subjected to bending. Bhashyam and Prathap [12] used Galerkin finite element method for nonlinear beam vibrations showing the main differences of the eigenvalue problems between linear and nonlinear vibrations. Lacarbonara *et al.* [13] performed nonlinear vibrations of buckled beams and made comparisons with analytical solution and experiments. Other researches were conducted in the field of free vibration, like the work of Fallah and Aghdam [14] about functionally graded beams, and the work of Asadi and Aghdam [15] about composite beams, for example.

The nonlinear analysis proposed in this work is based on the Carrera Unified Formulation (CUF) [16, 17], according to which any theory of structures can degenerate into a generalized kinematics that makes use of an arbitrary expansion of the generalized variables. In this manner, the nonlinear governing equations and the related finite element arrays of the generic geometrically-exact beam theory are written in terms of *fundamental nuclei*. These fundamental nuclei represent the basic building blocks that, when opportunely expanded, allow for the straightforward generation of low- and high-order finite beam elements. CUF has been utilized for many engineering problems over the last few years; e.g., composite structures [18], rotating blades and rotors [19], civil engineering structures [20], aerospace constructions [21, 22], and multi-field problems [23], among the others. CUF has been recently extended to geometric nonlinear problems, for both metallic and composite structure [24],[25]. Here, the formulation is further extended to deal with vibrations.

This paper is organized as follows: (i) first, some preliminary and introductory information are given in Section 2, including the constitutive expressions for elastic metallic materials, the Green-Lagrange nonlinear geometrical relations, CUF, and the related finite element; (ii) subsequently, Section 3 introduces the eigenvalue problem and briefly describes the *fundamental nuclei* of secant and tangent matrices. Moreover, it discusses the resolution of the vibration problem and explains the methodology applied in this work to investigate the evolution of the natural frequencies; (iii) then, numerical results are discussed for different loading and structural cases in Section 4; (iv) finally, the main conclusions are drawn.

2 Unified finite beam element

2.1 Preliminaries

Consider a beam structure whose cross-section Ω lays on the xz -plane of a Cartesian reference system. As a consequence, the beam axis is placed along y and measures L . The transposed displacement vector is introduced in the following:

$$\mathbf{u}(x, y, z) = \{ u_x \quad u_y \quad u_z \}^T \quad (1)$$

The stress, $\boldsymbol{\sigma}$, and strain, $\boldsymbol{\epsilon}$, components are expressed in vectorial form with no loss of generality,

$$\boldsymbol{\sigma} = \{ \sigma_{xx} \quad \sigma_{yy} \quad \sigma_{zz} \quad \sigma_{xz} \quad \sigma_{yz} \quad \sigma_{xy} \}^T, \quad \boldsymbol{\epsilon} = \{ \epsilon_{xx} \quad \epsilon_{yy} \quad \epsilon_{zz} \quad \epsilon_{xz} \quad \epsilon_{yz} \quad \epsilon_{xy} \}^T \quad (2)$$

In this work, linear elastic metallic beam structures are considered. Hence, the Hooke's law providing the constitutive relation holds as follows:

$$\boldsymbol{\sigma} = \mathbf{C}\boldsymbol{\epsilon} \quad (3)$$

where \mathbf{C} is the material matrix.

As far as the geometrical relations are concerned, the Green-Lagrange nonlinear strain components are considered. Therefore, the displacement-strain relations are expressed as

$$\boldsymbol{\epsilon} = \boldsymbol{\epsilon}_l + \boldsymbol{\epsilon}_{nl} = (\mathbf{b}_l + \mathbf{b}_{nl})\mathbf{u} \quad (4)$$

where \mathbf{b}_l and \mathbf{b}_{nl} are the linear and nonlinear differential operators, respectively. The complete form of these two matrices can be found in [24].

2.2 Carrera Unified Formulation

Within the framework of the Carrera Unified Formulation (CUF), the three-dimensional displacement field $\mathbf{u}(x, y, z)$ can be expressed as a general expansion of the primary unknowns. In the case of one-dimensional theories, one has:

$$\mathbf{u}(x, y, z) = F_s(x, z)\mathbf{u}_s(y), \quad s = 1, 2, \dots, M \quad (5)$$

where F_s are the functions of the coordinates x and z on the cross-section, \mathbf{u}_s is the vector of the *generalized* displacements which lay along the beam axis, M stands for the number of the terms used in the expansion, and the repeated subscript s indicates summation. The choice of F_s determines the class of the 1D CUF model that is required and subsequently to be adopted. The research work proposed in this paper makes use of nine-point polynomials to approximate the cross-sectional displacement field, and it is depicted in Fig. 1. As widely shown and demonstrated in [26] this approximated but refined kinematics can describe accurately a wide range of classes of structures.

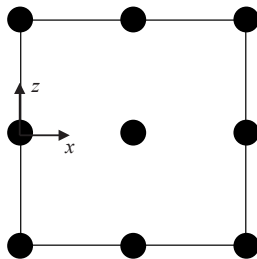


Figure 1: L9 polynomial cross-section

The displacement field given by one single L9 approximation is:

$$\begin{aligned} u_x &= F_1u_{x1} + F_2u_{x2} + F_3u_{x3} + F_4u_{x4} + F_5u_{x5} + F_6u_{x6} + F_7u_{x7} + F_8u_{x8} + F_9u_{x9} \\ u_y &= F_1u_{y1} + F_2u_{y2} + F_3u_{y3} + F_4u_{y4} + F_5u_{y5} + F_6u_{y6} + F_7u_{y7} + F_8u_{y8} + F_9u_{y9} \\ u_z &= F_1u_{z1} + F_2u_{z2} + F_3u_{z3} + F_4u_{z4} + F_5u_{z5} + F_6u_{z6} + F_7u_{z7} + F_8u_{z8} + F_9u_{z9} \end{aligned} \quad (6)$$

where u_{x1}, \dots, u_{z9} are the displacement variables of the problem. They represent the translational displacement components of each of the nine points of the L9 element. For further details on LE (Lagrange Expansion) models utilized in this paper, interested readers can refer to [26].

2.3 Finite element formulation

The Finite Element Method (FEM) is adopted to discretize the structure along the y axis. Thus, the generalized displacement vector $\mathbf{u}_s(y)$ is approximated as follows:

$$\mathbf{u}_s(y) = N_j(y)\mathbf{q}_{sj} \quad j = 1, 2, \dots, p + 1 \quad (7)$$

where N_j stands for the j -th shape function, p is the order of the shape functions and j indicates summation. \mathbf{q}_{sj} is the following vector of the FE nodal parameters:

$$\mathbf{q}_{sj} = \{ q_{u_{sj}} \quad q_{u_{sj}} \quad q_{u_{sj}} \}^T \quad (8)$$

For the sake of brevity, the shape functions N_j are not reported here. They can be found in many reference texts, for instance in Bathe [27]. However, it should be underlined that the choice of the cross-section polynomials sets for the LE kinematics (i.e. the selection of the type, the number and the distribution of cross-sectional polynomials) is completely independent of the choice of the beam finite element to be used along the beam axis. In this work, classical one-dimensional finite elements with four nodes (B4) are adopted, i.e. a cubic approximation along the y axis is assumed.

3 Free vibrations of nonlinear structures

3.1 Secant and tangent stiffness matrices

Equations of motion of an elastic body undergoing undamped free vibrations can be obtained with ease by using the principle of virtual work, which in this case states that:

$$\delta L_{\text{int}} - \delta L_{\text{ine}} = 0 \quad (9)$$

where L_{int} stands for the strain energy, L_{ine} is the work of the inertial loads, and δ represents the virtual variation operator. Given the stress ($\boldsymbol{\sigma}$) and strain ($\boldsymbol{\epsilon}$) vectors, the virtual variation of the internal strain energy can be written as

$$\delta L_{\text{int}} = \langle \delta \boldsymbol{\epsilon}^T \boldsymbol{\sigma} \rangle \quad (10)$$

where $\langle \cdot \rangle = \int_V (\cdot) dV$. Under the hypothesis of small deformations, $V = \Omega \times L$ is the initial volume of the beam structure. Introducing the CUF (Eq. 5) and FEM (Eq. 7) relations into Eq. 4, the strain vector can be written in algebraic form as follows:

$$\boldsymbol{\epsilon} = (\mathbf{B}_l^{sj} + \mathbf{B}_{nl}^{sj})\mathbf{q}_{sj} \quad (11)$$

where \mathbf{B}_l^{sj} and \mathbf{B}_{nl}^{sj} are the linear and nonlinear algebraic matrices with CUF (Eq. 5) and FEM (Eq. 7) formulations.

Substituting the Eq. 11 and the constitutive equations for elastic materials (Eq. 3) into Eq. 10, one has:

$$\begin{aligned}
\delta L_{\text{int}} &= \delta \mathbf{q}_{\tau i}^T \langle (\mathbf{B}_l^{\tau i} + 2\mathbf{B}_{nl}^{\tau i})^T \mathbf{C} (\mathbf{B}_l^{sj} + \mathbf{B}_{nl}^{sj}) \rangle \mathbf{q}_{sj} \\
&= \delta \mathbf{q}_{\tau i}^T \mathbf{K}_0^{ij\tau s} \mathbf{q}_{sj} + \delta \mathbf{q}_{\tau i}^T \mathbf{K}_{lnl}^{ij\tau s} \mathbf{q}_{sj} + \delta \mathbf{q}_{\tau i}^T \mathbf{K}_{nll}^{ij\tau s} \mathbf{q}_{sj} + \delta \mathbf{q}_{\tau i}^T \mathbf{K}_{nlnl}^{ij\tau s} \mathbf{q}_{sj} \\
&= \delta \mathbf{q}_{\tau i}^T \mathbf{K}_S^{ij\tau s} \mathbf{q}_{sj}
\end{aligned} \tag{12}$$

where the secant stiffness matrix is $\mathbf{K}_S^{ij\tau s} = \mathbf{K}_0^{ij\tau s} + \mathbf{K}_{lnl}^{ij\tau s} + \mathbf{K}_{nll}^{ij\tau s} + \mathbf{K}_{nlnl}^{ij\tau s}$. In Eq. 12, $\mathbf{K}_0^{ij\tau s}$ is the linear component of \mathbf{K}_S (i.e., it is the linear stiffness matrix), $\mathbf{K}_{lnl}^{ij\tau s}$ and $\mathbf{K}_{nll}^{ij\tau s}$ represent the nonlinear contributions of order 1, and $\mathbf{K}_{nlnl}^{ij\tau s}$ contains the nonlinearities of order 2. These are the fundamental nuclei (FN), which 3 x 3 matrices that, given the theory approximation order (i.e., given the cross-sectional functions ($F_\tau = F_s$, for $\tau = s$) and the shape functions ($N_i = N_j$, for $i = j$), can be expanded by using the indexes $\tau, s = 1, \dots, M$ and $i, j = 1, \dots, p+1$ in order to obtain the element stiffness matrices of any arbitrarily refined beam model. In other words, by opportunely choosing the beam kinematics, classical to higher-order beam theories and related stiffness array can be implemented in an automatic manner by exploiting the index notation of CUF. The explicit derivation of the stiffness FN is not provided here for the sake of brevity, but it can be found in [24]. In a similar manner, the FN of the linear mass matrix can be obtained from the virtual variations of the inertial loadings as follows:

$$\delta L_{\text{ine}} = \langle \delta \mathbf{q}^T \boldsymbol{\rho} \ddot{\mathbf{q}} \rangle = \delta \mathbf{q}_{sj}^T \mathbf{M}^{ij\tau s} \ddot{\mathbf{q}}_{\tau i} \tag{13}$$

where $\mathbf{M}^{ij\tau s}$ is the FN of the mass matrix. It is fairly obvious that the modal behavior of any system is a property of the equilibrium, and not merely of the structure geometrical/mechanical characteristics. Inherently, free vibration analysis needs to be made about a linearized equilibrium state along the equilibrium path. For this purpose, Eq. 9 needs to be properly linearized in order to obtain the modal behaviour of the structure about given states of the equilibrium path. Assuming as linear the virtual variation of the inertial work, we need to linearize the virtual variation of the nonlinear, internal strain energy to obtain the tangent stiffness matrix (for a deeper treatment of the topic, see [24]):

$$\begin{aligned}
\delta(\delta L_{\text{int}}) &= \langle \delta(\delta \boldsymbol{\epsilon}^T \boldsymbol{\sigma}) \rangle \\
&= \langle \delta \boldsymbol{\epsilon}^T \delta \boldsymbol{\sigma} \rangle + \langle \delta(\delta \boldsymbol{\epsilon}^T) \boldsymbol{\sigma} \rangle \\
&= \delta \mathbf{q}_{\tau i}^T (\mathbf{K}_0^{ij\tau s} + \mathbf{K}_{T_1}^{ij\tau s} + \mathbf{K}_\sigma^{ij\tau s}) \delta \mathbf{q}_{sj} \\
&= \delta \mathbf{q}_{\tau i}^T \mathbf{K}_T^{ij\tau s} \delta \mathbf{q}_{sj}
\end{aligned} \tag{14}$$

where $\mathbf{K}_{T_1}^{ij\tau s} = 2\mathbf{K}_{lnl}^{ij\tau s} + \mathbf{K}_{nll}^{ij\tau s} + 2\mathbf{K}_{nlnl}^{ij\tau s}$ is the nonlinear contribution of the fundamental nucleus of the tangent stiffness matrix due to the linearization of the Hooke's law. $\mathbf{K}_0^{ij\tau s}$, $\mathbf{K}_{lnl}^{ij\tau s}$, $\mathbf{K}_{nll}^{ij\tau s}$, and $\mathbf{K}_{nlnl}^{ij\tau s}$ are the same 3×3 FNs as given in Eq. 12. \mathbf{K}_σ comes from the linearization of the nonlinear form of the strain-displacement equations and is often called the *geometric stiffness*.

3.2 Linearized eigenvalue problem

By using Eqs. 14 and 13 into the linearization of Eq. 9 and assuming harmonic displacements, the equations of motion for free vibrations hold the form of a linear eigenvalue problem, which in unified form reads:

$$(\mathbf{K}_T^{ij\tau s} - \omega^2 \mathbf{M}^{ij\tau s}) \mathbf{q}_{\tau i} = 0 \quad (15)$$

where ω is a natural period and $\mathbf{q}_{\tau i}$ the related amplitude eigenvecture.

This formulation comports some simplifications; important aspects should be underlined for the sake of completeness:

- The accuracy of the proposed methodology, of course, depends on the capability of the structural theory to describe nonlinear analysis in an accurate manner, which is the case of the present CUF methodology.

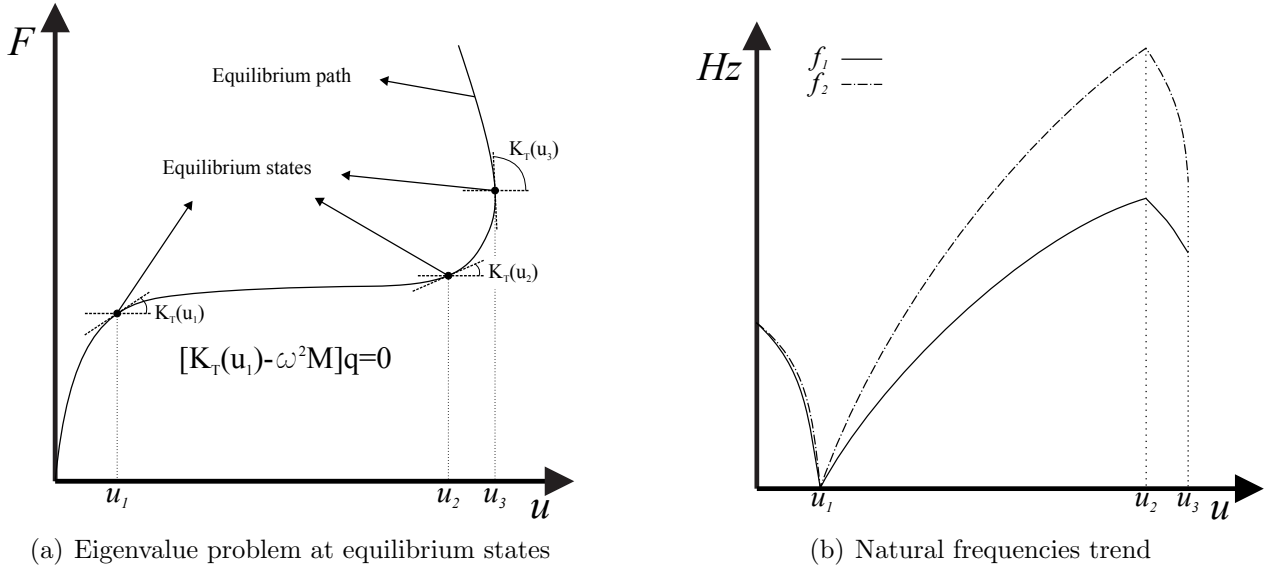


Figure 2: Natural frequencies evaluation from eigenvalue problems solving about some equilibrium states of nonlinear equilibrium path.

- The nonlinear vibrations have low amplitudes, so the linearization around some states of the equilibrium path and the assumption of harmonic oscillations are legit.
- Inertial work is neglected in the evaluation of the equilibrium path.
- The proposed method is able to identify bifurcations, elastic instabilities or buckling phenomena as those conditions which render the tangent stiffness matrix singular, see Fig. 2.

4 Numerical results

In this section, various problems are addressed for demonstrating: 1) how large deflection fields and rotations affect the natural frequencies; 2) the enhanced capabilities of the proposed nonlinear refined formulation. Large deflection and *elastica-like* analyses of one-dimensional solid cross-section structures are considered. Here, the attention is focussed on the capability of the proposed geometrically nonlinear CUF beam model to account for natural frequencies evaluation in a unified framework. For the cases analyzed, two kinds of section are considered, square cross-section and thin-walled unsymmetric C-section. Also two loading conditions, i.e. bending and compression. Regarding bending on square cross-section beam, both short and slender beam are considered.

4.1 Cantilever beams subjected to flexure

In the first analysis case, a cantilever, square cross-section beam subjected to large deflection due to a transverse loading is considered. The beam is made of an aluminum alloy with Young modulus E equal to 75 GPa and Poisson ratio $\nu = 0.33$, and is subjected to clamped-free boundary conditions. A loading P is applied at the free end as shown in Fig. 3. Two beams are considered with the same cross-section but with two different lengths, $L_1 = 2m$ and $L_1 = 20m$. In all the analyses, the side of the cross-section, $w = 20mm$, remains unchanged in order to simulate both thick and slender beams. For all the subsequent discussions, 20 cubic beam elements are used along the longitudinal axis, whereas one single $L9$ polynomial is used to approximate the theory kinematics on the cross-section. This model was already validated in [24] for static response nonlinear analysis.

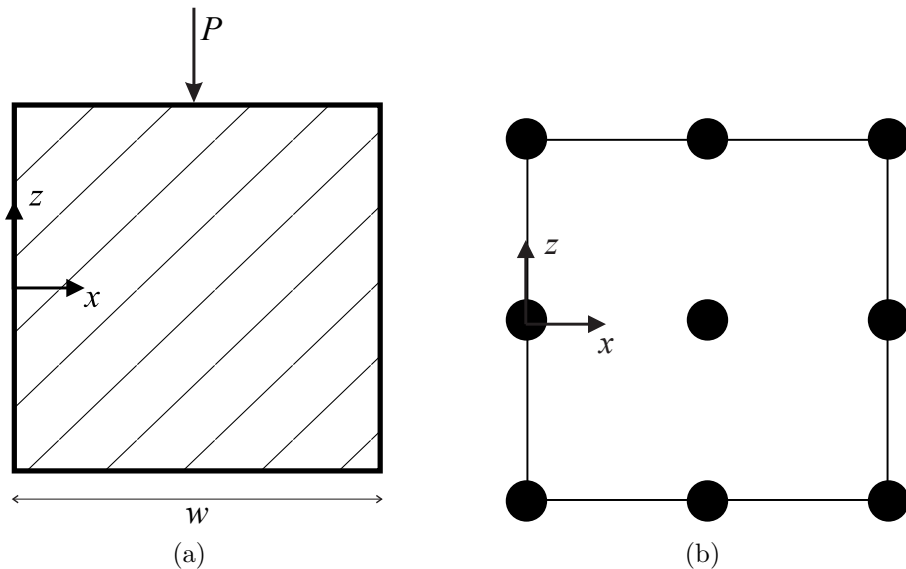


Figure 3: Cross-section geometry (a) and discretization with 1L9 Lagrange polynomials (b) of the unsymmetric channel beam and loading condition.

Fig. 4 shows the equilibrium curves for short and slender beam structures, and the results of the present beam model are compared to those from linear and nonlinear Euler-Bernoulli beam models. From the solution iterates (circles in Fig. 4), it is clear that an arc-length method is used to find the equilibrium curves of the 1L9 beam model. In the figure, also the equilibrium deformation of some nonlinear analysis steps are depicted.

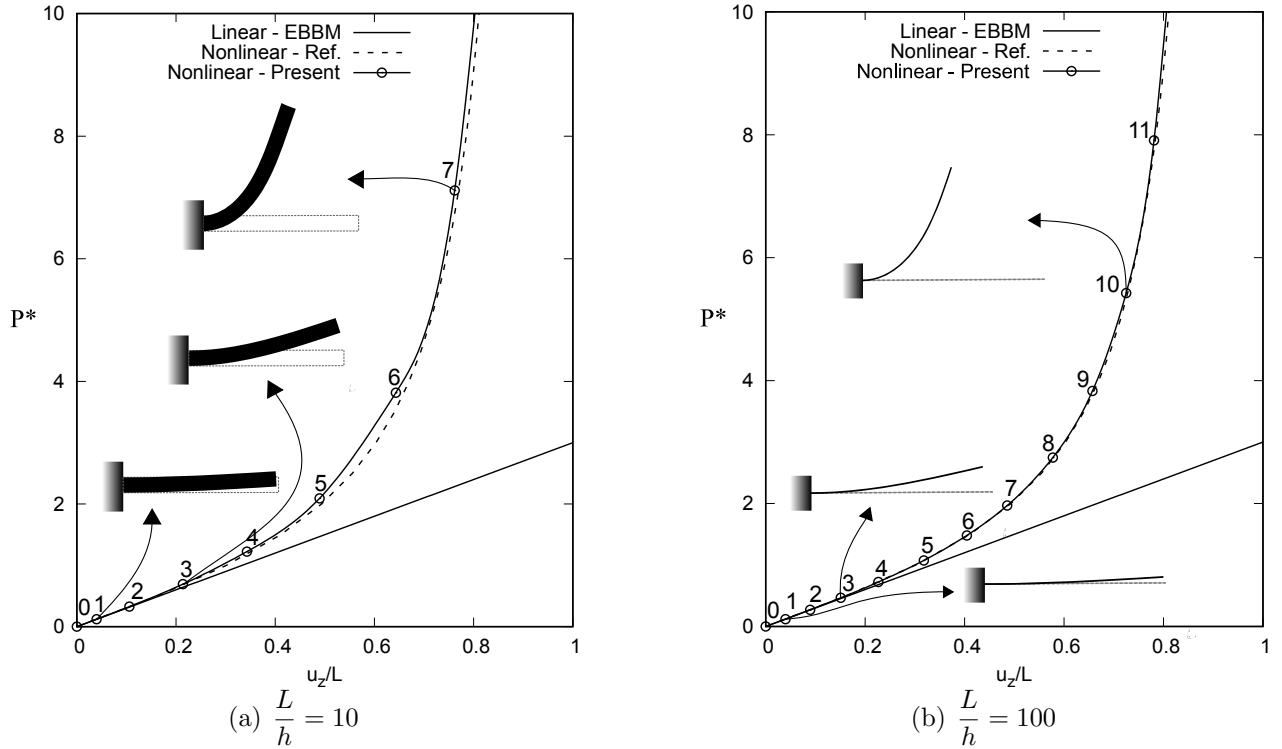


Figure 4: Equilibrium curves of the square cross-section beam subjected to vertical loading. Reference solution from [28]. $P^* = \frac{l^2}{EI}$

The natural frequencies of the nonlinear analysis are analyzed subsequently. At each step of the analysis, free vibrations are evaluated as described in Section 3 and by using the local tangent stiffness of the deformed structure. Table 1 and Table 2 show the values of the natural frequencies for two bending and one torsional modal shapes, for both short and slender beams. Step numbers are referred to Fig. 4. In the case of short beam, these modes are the 1st, 2nd and 5th ones, while in the slender beam case they are the respectively modes 1st, 2nd and 13th. The values of the bending natural frequency increase as the load rises, for both short and slender beam. Furthermore, considering that the applied load is along the z axis, the natural frequency of the bending mode along this axis (the fourth column of the tables) increases more than the frequency associated to the bending mode along x . This aspect is mainly due to the fact that the stress concentration caused by the external load has the same nature (and direction) of the one caused by the modal shape. In other words, the nonlinear geometric stiffness \mathbf{K}_σ due to the external load directly affects the bending mode along z . On the other hand, as far as the bending mode along x is concerned (the third column of the tables), the applied load and the modal shape have different directions, so their stress fields are not strongly related each other; thus, geometric nonlinear effects on this mode are less considerable, see Fig. 5. The natural frequency of the bending modal shape with the same direction of the applied external load increases by the 123.37% for the short beam and by the 142.39% for the slender beam. In contrast, for the bending mode along x , the percentages of variation are lower, 107.56% for the short beam and 120.84% for the slender beam, as highlighted in Fig. 6

For the sake of completeness, Fig. 7 shows the variation of the first 10 natural frequencies as function of the beam tip deflection. It can be pointed out that the trends of the short and

$L/h = 10$				
				
$Step$	u_z/L	f_1	f_2	f_3
0	0.000	42.56	42.56	403.9
1	0.040	42.66	42.80	406.3
2	0.106	43.31	43.98	415.6
3	0.214	43.41	44.41	410.7
4	0.343	44.92	47.08	414, 5
5	0.489	48.11	52.09	418.8
6	0.643	54.67	61.15	420.9
7	0.762	65.78	74.49	421.4
8	0.851	88.39	95.89	521.6

Table 1: Natural frequencies (Hz) values at various steps of the nonlinear analysis for bending modes and torsional mode. Short beam case.

$L/h = 100$				
				
$Step$	u_z/L	f_1	f_2	f_3
0	0.000	0.427	0.427	40.39
1	0.039	0.427	0.427	40.41
2	0.089	0.428	0.430	40.43
3	0.151	0.431	0.435	40.47
4	0.227	0.437	0.445	40.53
5	0.318	0.448	0.462	40.54
6	0.405	0.463	0.486	40.56
7	0.487	0.484	0.519	40.77
8	0.577	0.525	0.573	42.27
9	0.657	0.613	0.670	51.63
10	0.725	0.720	0.789	65.33
11	0.781	0.839	0.921	79.48
12	0.827	0.943	1.035	79.95

Table 2: Natural frequencies (Hz) values at various steps of the nonlinear analysis for bending modes and torsional mode. Slender beam case.

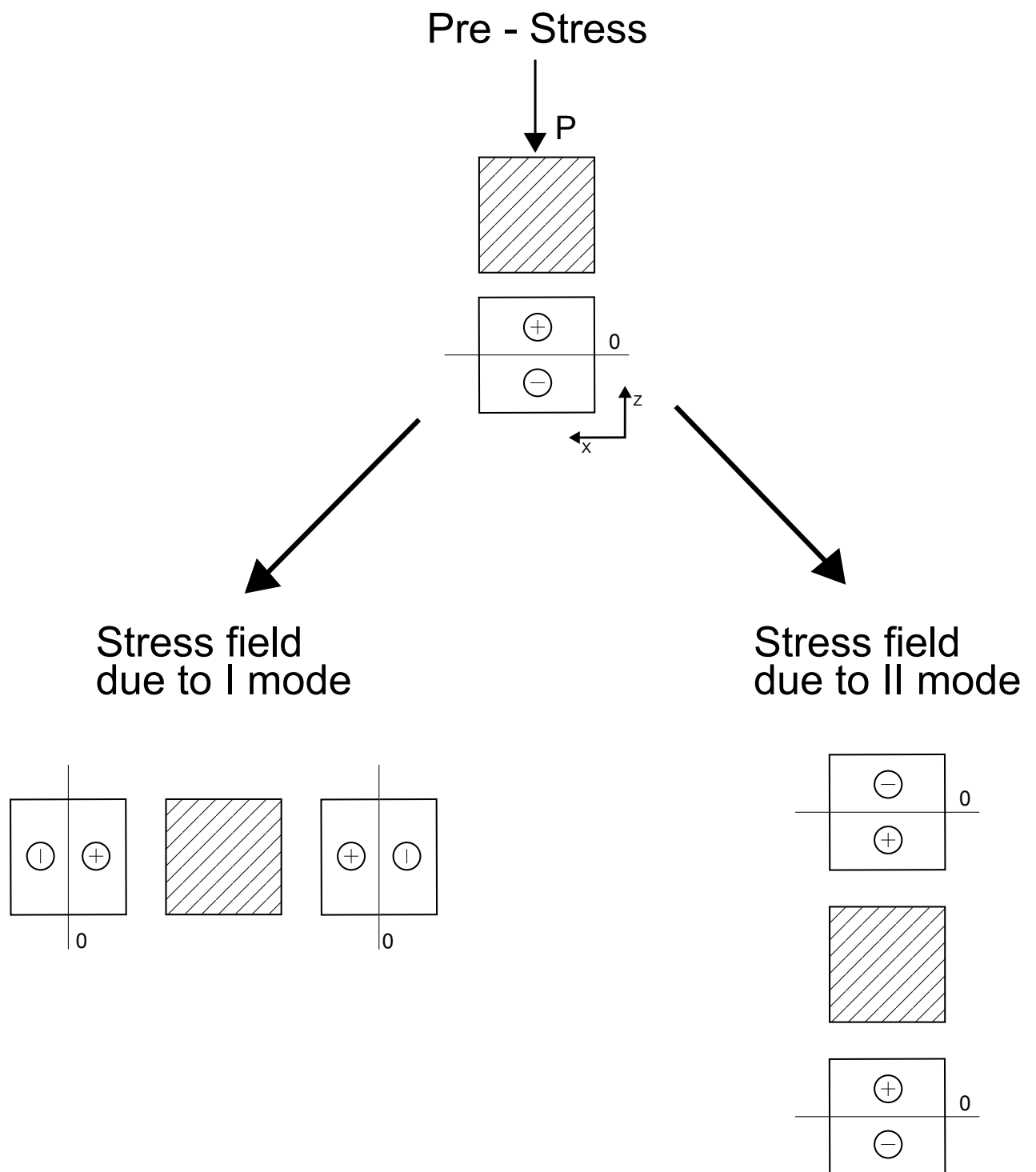


Figure 5: Stress fields on beam section due to both external load (pre-stress) and modal shape. Plus sign stands for traction, minus sign for compression.

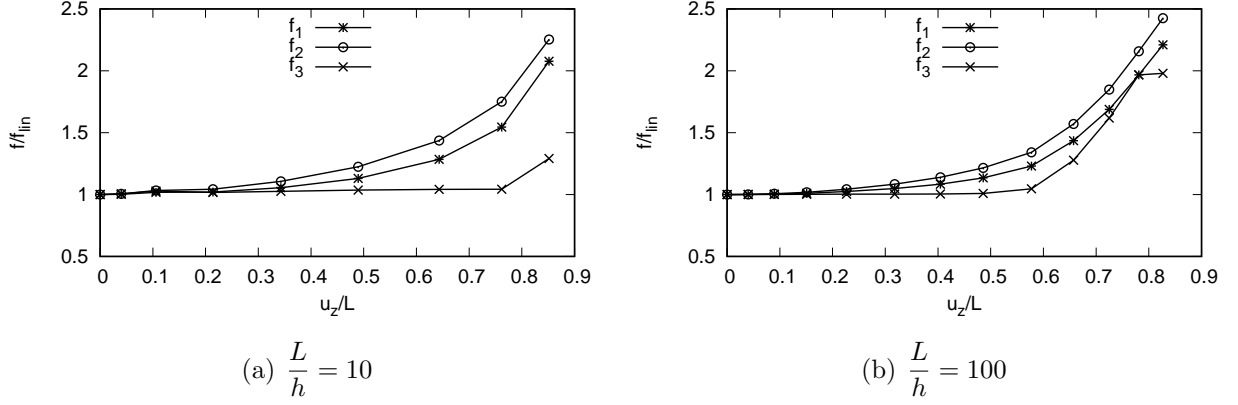


Figure 6: Natural frequencies trend of first two bending modes and torsional mode for both short (a) and slender (b) beam. The frequency is adimensionalized with the correspondent linear frequency to highlight the growth due to the increase of the external load.

the slender beams are different. For the thick beam it can be observe a more irregular trend. The first two couples of modes (f_1, f_2 and f_3, f_4) change their frequencies values when the vertical displacement is between 20% and 30% of the length of the beam, which is the same value when the beam start to have a nonlinear behavior (as it can be observed in Fig. 4). All the natural frequencies increase at higher steps of the nonlinear analysis, except f_6 , which is the axial one. In addition, f_6 and f_8 start to change from the first steps of the analysis, where the beam has a linear behavior trend. About the slender beam, each couple of normal modes has almost the same behavior, starting to change when the vertical displacement reaches the 30%-35% of the length of the beam. In this case, in fact, the first modes are dominated by bending, and axial/shear modes are not present.

To trace the trend of the natural frequency of the torsional modal shape, higher modes must be analyzed, see Fig. 8. As the analysis goes on and the applied load increases, the frequency of the torsional mode has a regular trend until the value of the adimensionalized displacement reaches the value of 0.6. Then, the torsional frequency starts to increase and is affected by crossing phenomena.

In Fig. 9, significant MAC (Modal Assurance Criterion) graphical representations are reported. MAC is a scalar representing the comparison and correspondence between two sets of mode shapes. Significant steps of the nonlinear analysis are considered, and they are all related to the step 0, which represents the linear case. For the short beam (Fig. 9a), the three figures compare the first 10 modes for progressively increasing displacement configurations, from nearly-linear (step 1 of the analysis) to moderate (step 3) and highly-nonlinear (step 7). As shown from the figures, natural modes in the case of low load (step 1, first of the three figures in Fig. 9a) are very similar to those related to the linear case: black boxes are only in the diagonal. There are some grey boxes for the modes 8 and 10 and this denotes that the behavior slightly differs from the linear one. Step 3 starts to be different from step 0, and dark boxes appears in other spots of the grid, which indicates that the beam has a concrete different behavior from the linear theory. Finally, in step 7, the state is completely nonlinear, and dark boxes appears spread within the grid.

The same approach is repeated for the slender beam, where the last step considered is the 10th. First two figures are very similar each other: in fact, until step 3 the beam's behavior is very close to the linear one. The last figure suggests a nonlinear behavior.

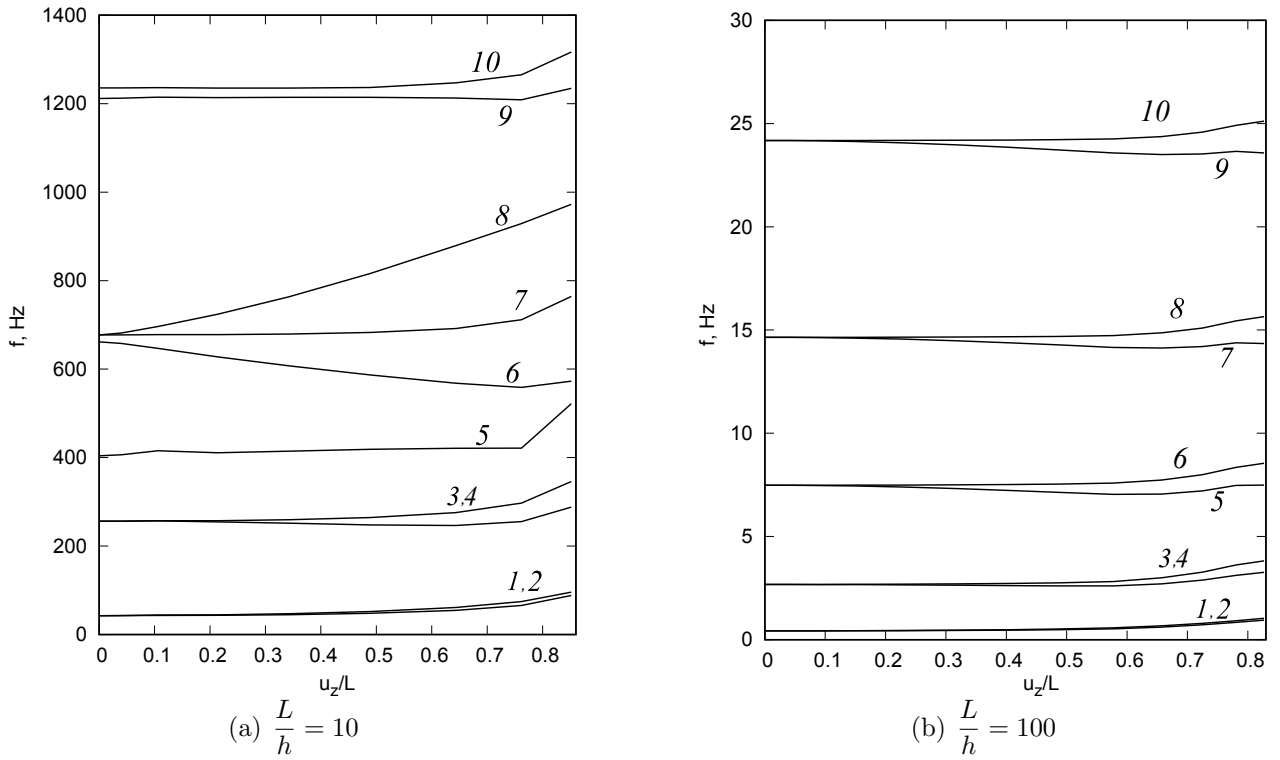


Figure 7: First 10 natural frequencies trends for both thick and slender beam.

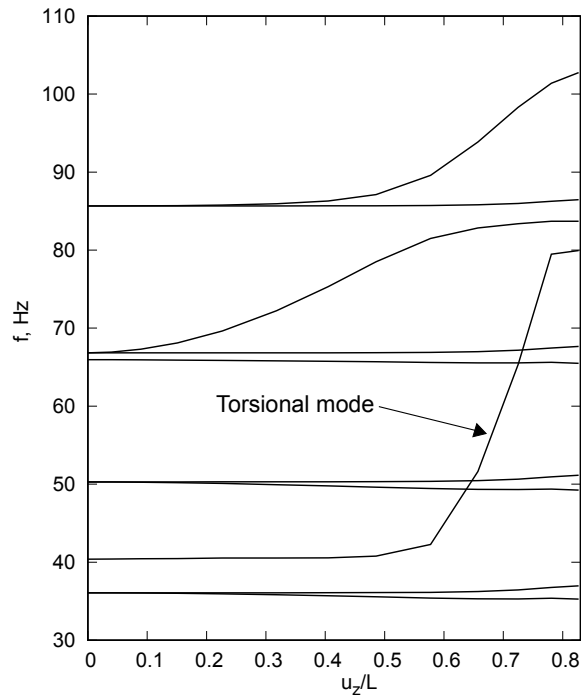


Figure 8: Natural frequencies trend of modal shapes from 10 to 20 of slender beam. The first torsional mode is highlighted.

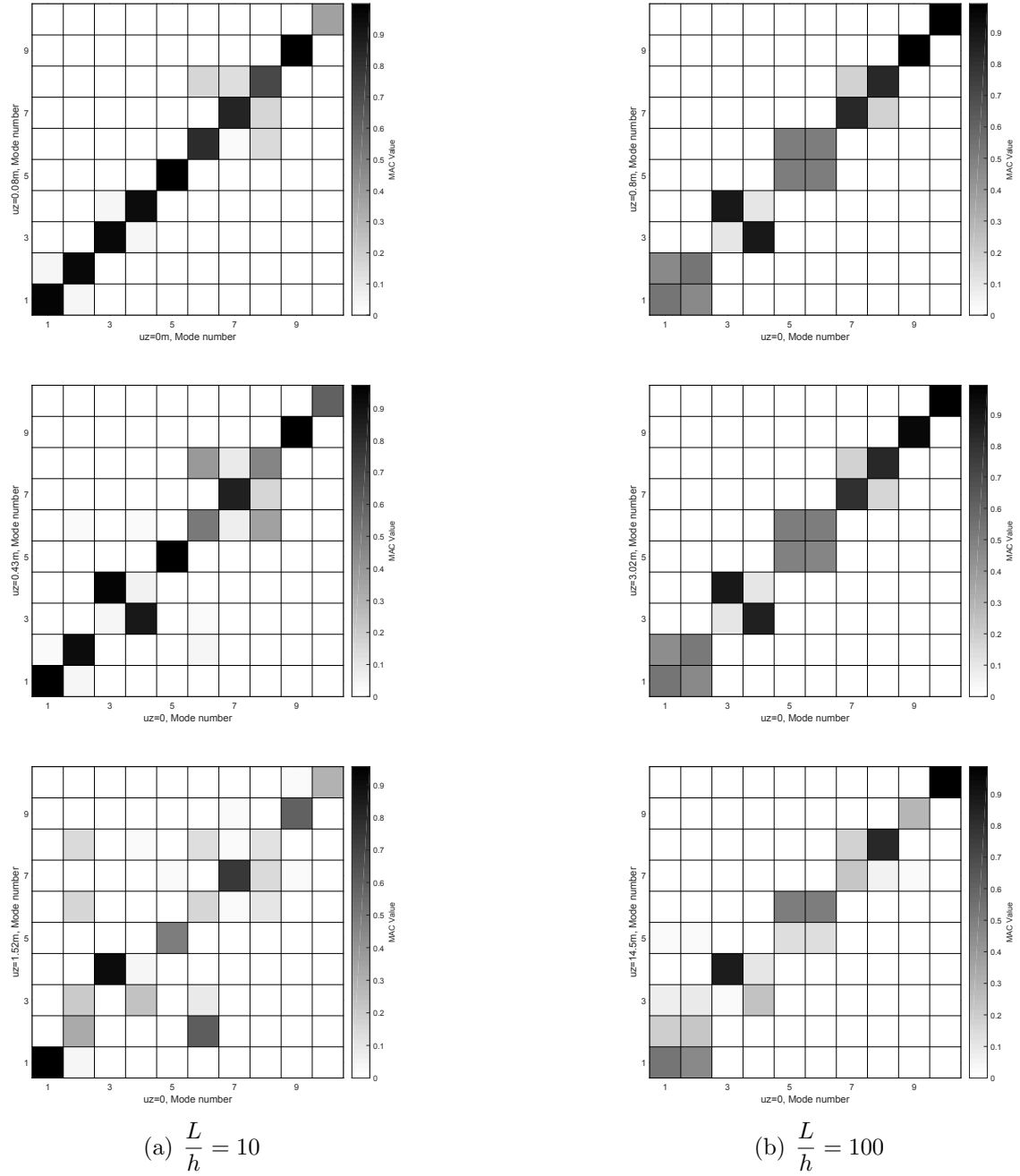


Figure 9: Values of MAC between the modes of the undeformed structure and those of the deformed structure for both thick and slender beam.

4.2 Post-buckling of beam-columns

The post-buckling behavior of the same slender beam structure (Fig. 3) as considered in the previous analysis case is addressed. Post-buckling curve of the clamped-free configuration $L/h = 100$ is shown in Fig. 10, which gives the transverse displacement versus the loading P according to the high-order 1L9 beam model. It must be clarified that the displacement is measured at the free end. The unstable solution branches have been *enforced* by applying a small load defect d as depicted in the figure and the arc-length method has been employed.

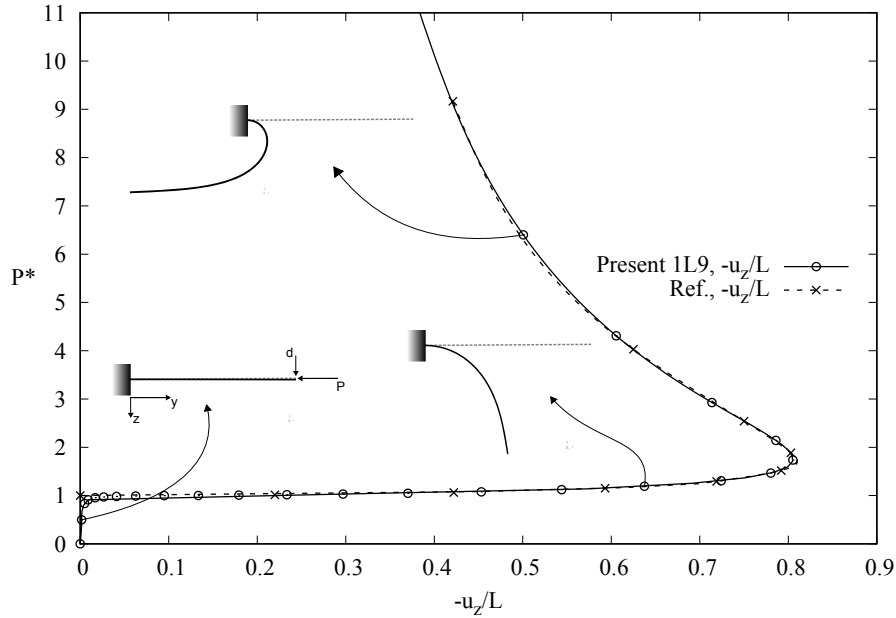


Figure 10: Equilibrium curves of the square cross-section beam subjected to compression loading. $P^* = \frac{4L^2}{\pi^2 EI}$

Then, in each step of the nonlinear analysis, highlighted by circles in Fig. 10, first 10 natural frequencies of modal shapes were calculated. Table 3 shows the values of natural frequencies of the first 10 modes of this case at significant steps (whose numbering refers to Fig. 10).

Fig. 11 shows natural frequencies trends for the first 4 modal shapes. An interesting fact is the oscillating behavior of the first natural frequency. This is also clear from the Table 3: the frequency of the MODE 1 has his minimum value at step 12, $0.025Hz$, it grows up until step 16 to $0.193Hz$, decreased to $0.030Hz$ of the 17th step, and increase to $0.301Hz$ on the step 21. This particular behavior of the natural frequency value could be explained looking at stress fields on the beam during the overall analysis. In fact stress condition due to external loading changes continuously: from total compression stress in the first step, to more complex stress condition in the last step, which consists in traction/compression, compression/traction and full traction stress simultaneously. This means that the stress condition keep changing during the deformation, and in particular what is changing is the position of the neutral axis on the cross-section of the beam. In fact, when the beam is post-buckled, the loading condition is (analogously to the stress condition) similar to a bending case. Hence, neutral axis appears (from the total compression stress condition in the beam before buckling) and, as the structure buckles, the traction condition fraction increases in the beam section. The trend of the neutral axis coordinate increasing, as the external load is applied, is shown in Fig. 12. The figure shows the trend at 3 different sections of the beam: at $L/6$, at $L/2$ and at L . One thing that has to be highlighted is the fact that the neutral axis coordinate at $y = L$ goes

<i>Step</i>	$-u_z/L$	<i>MODE</i>					
		1	2	3	4	5	6
		f_1	f_2	f_3	f_4	f_5	f_6
0	0.000	0.427	0.427	2.674	2.674	7.481	7.481
1	0.033	0.308	0.308	2.561	2.561	7.387	7.387
2	0.100	0.178	0.178	2.481	2.481	7.322	7.322
3	0.180	0.135	0.135	2.465	2.465	7.309	7.309
4	0.340	0.098	0.098	2.454	2.454	7.300	7.300
5	0.532	0.078	0.079	2.449	2.450	7.296	7.297
6	0.821	0.063	0.065	2.446	2.447	7.292	7.295
7	1.253	0.051	0.055	2.443	2.446	7.286	7.293
10	3.586	0.030	0.070	2.422	2.444	7.232	7.291
11	4.669	0.026	0.087	2.407	2.445	7.191	7.290
12	5.939	0.025	0.110	2.385	2.446	7.132	7.288
15	10.88	0.106	0.239	2.267	2.472	6.802	7.291
16	12.75	0.193	0.328	2.227	2.517	6.657	7.310
17	14.48	0.030	0.330	2.097	2.478	6.411	7.272
21	14.27	0.301	0.746	1.967	2.753	5.880	7.428
22	24.18	0.457	0.929	2.087	3.018	6.037	7.678

Table 3: Natural frequencies (Hz) values at most significant steps of the nonlinear analysis for the first 6 modes.

from positive to negative after the beam is buckled, while in the other sections of the beam this coordinate is 0. All this continuous change on the stress condition over the cross-section of the beam causes the natural frequencies trend shown in Fig. 11.

To better understand the complicated stress field evolution in the beam subjected to a compression load, in Fig. 13 the stress field of three section of the beam is shown, together with the position of the coordinate of the neutral axis of the beam. The result is that the stress field continues to change in the beam, going from a traction-compression case (neutral axis coordinate equal to 0) to a full compression case (neutral axis coordinate equal to -0.1). Section C has a parabolic trend because the external load is applied as a single force at the center of the section.

4.3 Thin-walled channel-section beams

As a final example, thin-walled unsymmetric C-section cantilever beam structure is addressed. The beam is made of the same aluminium alloy as in the previous sections ($E = 75GPa$, $\nu = 0.33$), it is $1m$ long, and is subjected to clamped-free boundary conditions. A loading P is applied at the free end as shown in Fig. 14. According to this figure, which also shows the cross-sectional dimensions, $b = 100mm$, $h_1 = 48mm$, $h_2 = 88mm$, and $t = 8mm$, 7 quadratic L9 polynomials are employed to discretize the beam kinematics on the cross-section and, on the other hand, 20 B4 beam elements are used along the beam axis.

Fig. 15 shows both linear and nonlinear trends of the z -coordinate displacement of point A, previously shown in Fig. 14. In addition, the deformation of the beam are depicted for initial, middle and final steps of the nonlinear analysis. As can be seen from the figure, in step 9 the beam rotates, and this has consequences on the evolution of the modal shapes, as will be highlighted later. Fig. 16 and Table 4 show natural frequencies trends and values,

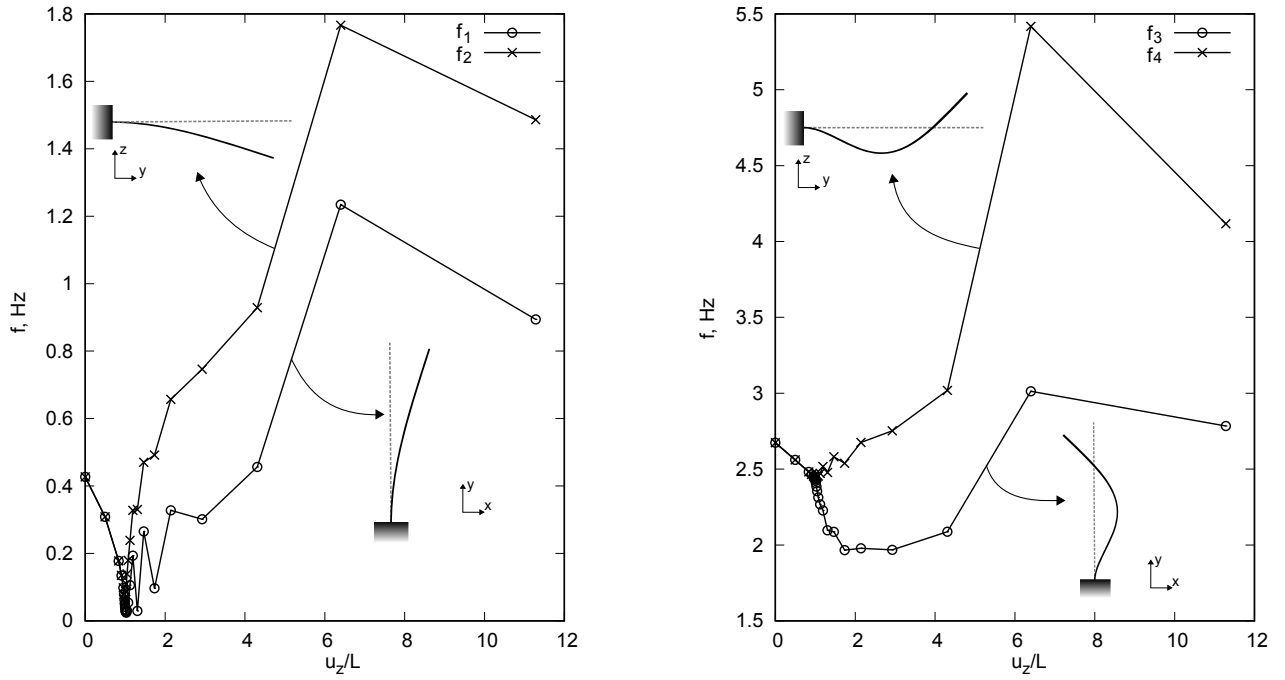


Figure 11: Natural frequencies trend for compression loaded beams for the first 4 modes.

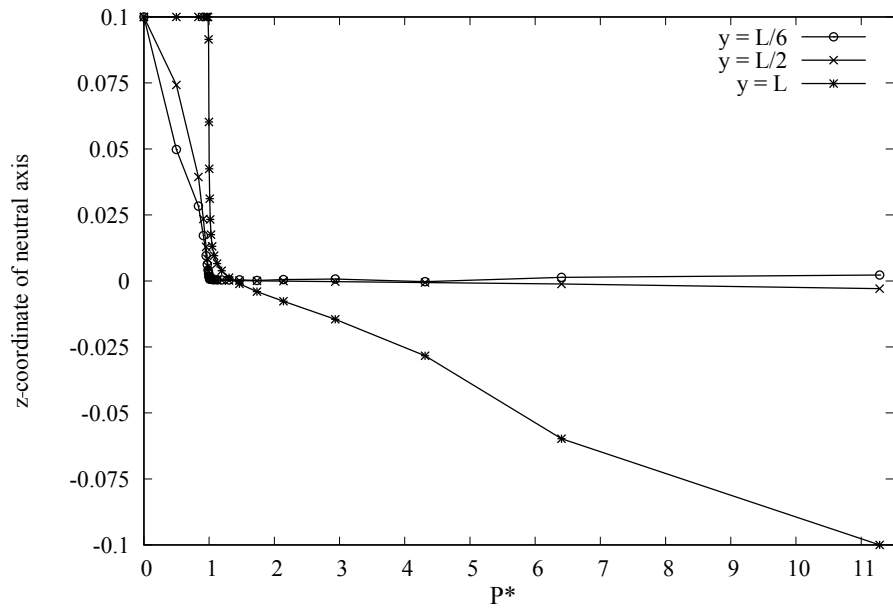


Figure 12: Neutral axis coordinate over the cross-section of the beam. $P^* = \frac{PAL^2}{\pi^2 EI}$

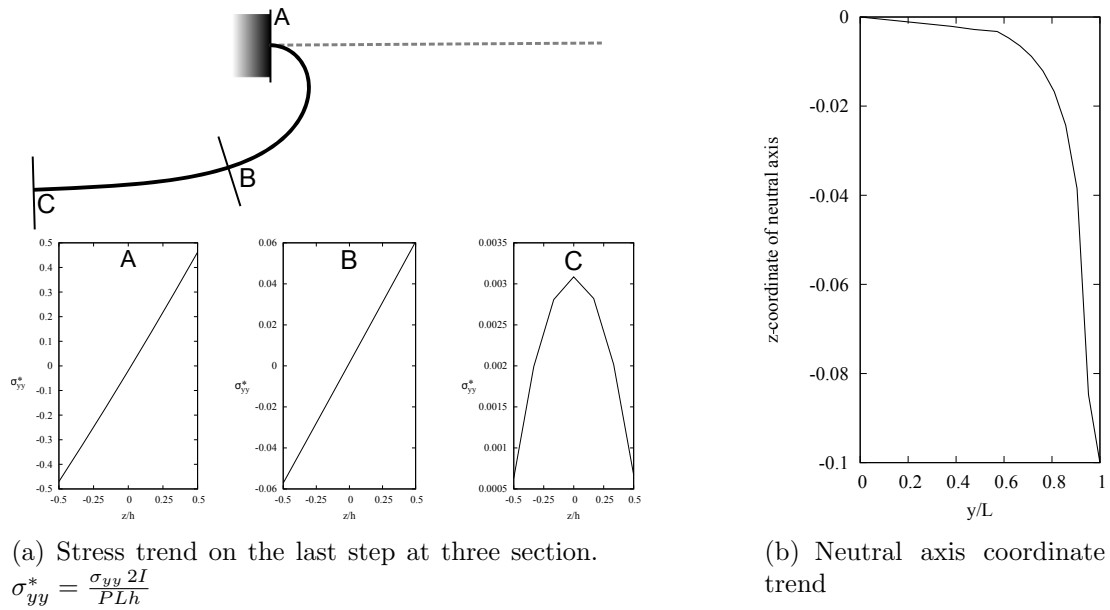


Figure 13: Stress field and neutral axis coordinate for the last step of the nonlinear analysis of the compression loading case.

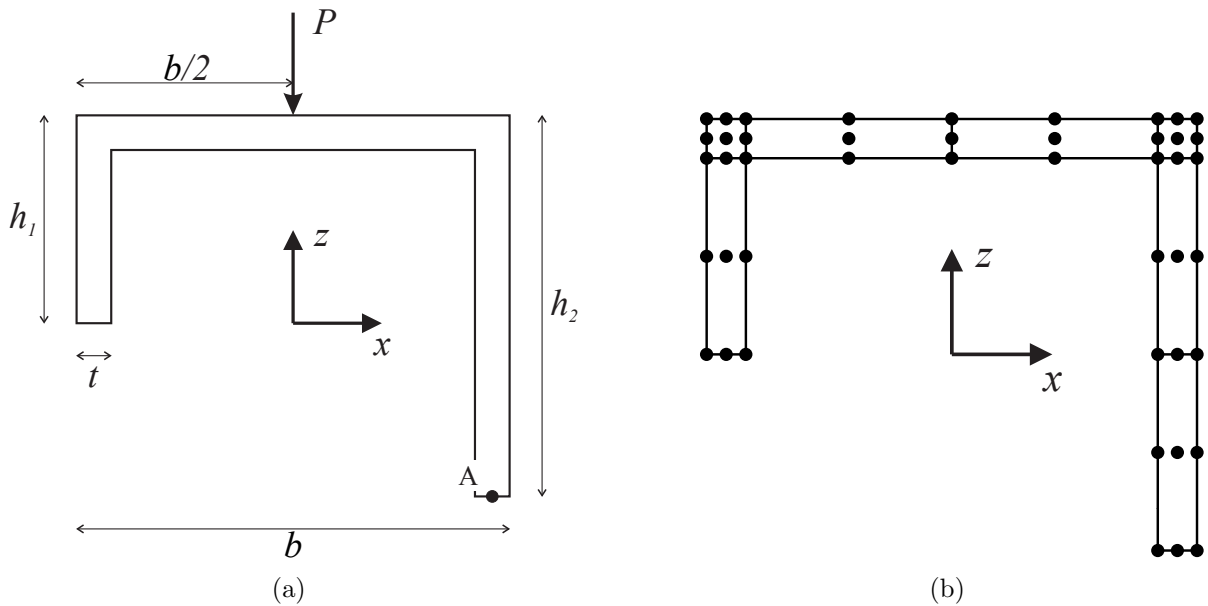


Figure 14: Cross-section geometry (a) and discretization with 7L9 Lagrange polynomials (b) of the unsymmetric channel beam.

respectively, of the first 5 modes. As can be seen from the figure, natural frequencies of the first two modal shapes have a more regular trend than the other three modes. Although this phenomena, modal shapes of first two modes are changing at progressive steps of the analysis. Fig. 17 and Fig. 18 show modal shapes at various step of the analysis: it can be observed that due to the fact that the beam rotates, modal shapes drastically change.

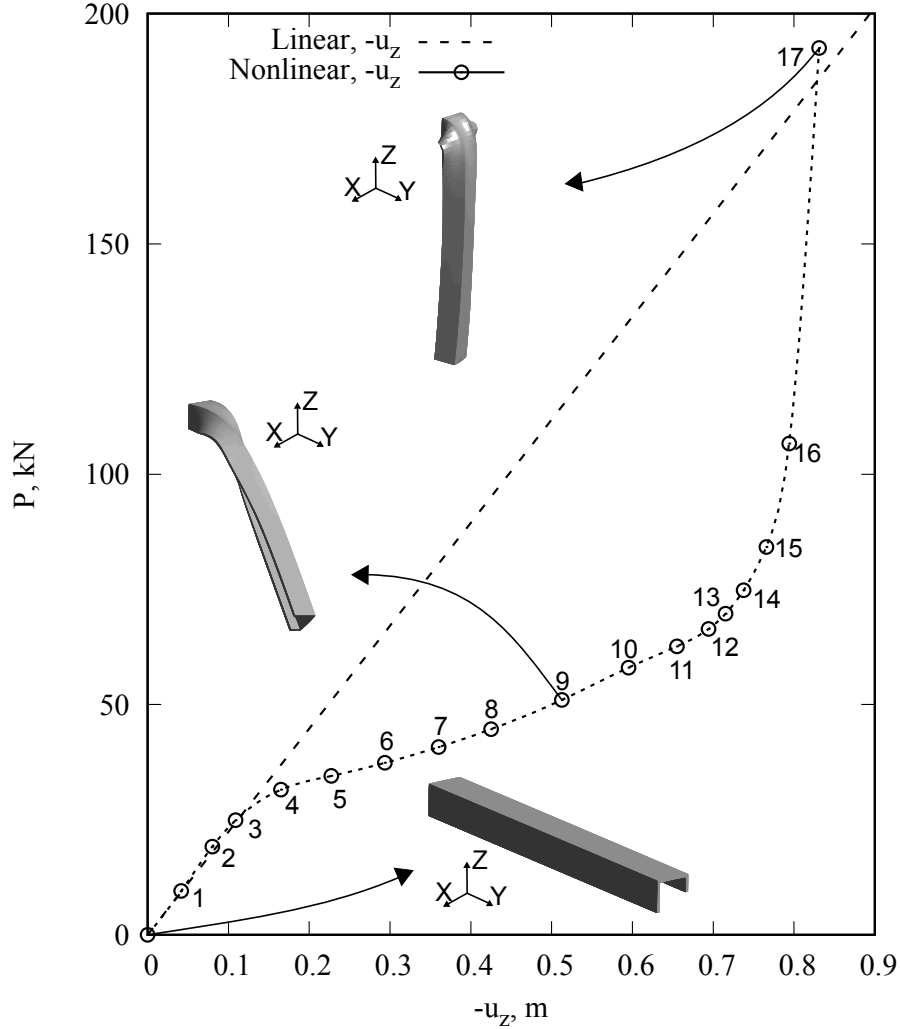


Figure 15: Displacement z component at point A on the tip cross-section vs. load. Behavior of the unsymmetric C-section beam in the large displacement range, with both linear and nonlinear LE beam models.

5 Conclusions

The unified formulation of geometrically nonlinear and elastic beam theory has been briefly introduced and utilized in this work. By employing the Carrera Unified Formulation (CUF), the nonlinear governing equations and the related finite element approximation have been formulated using the principle of virtual work. Nonlinear vibrations method have been employed to investigate natural frequencies evolution in nonlinear analysis, by linearizing some equilibrium states on the nonlinear equilibrium path of certain structures. The results related to solid as well as thin-walled cross-section beam structures have widely demonstrated the versatility of the proposed methodology and a not negligible changing of the modal shapes

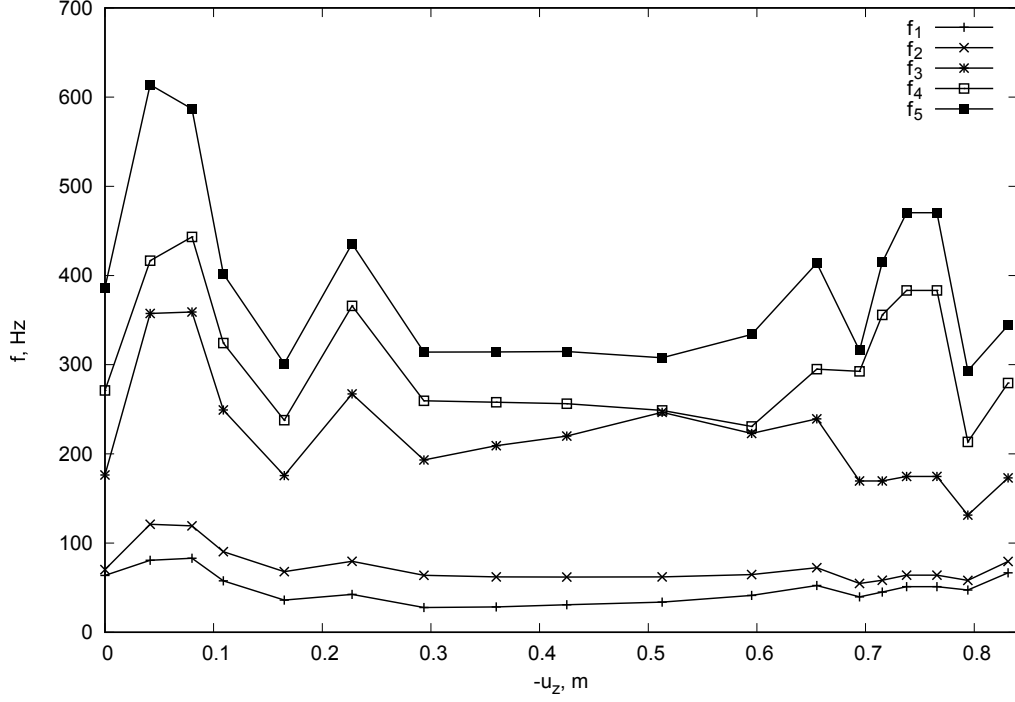


Figure 16: First 5 natural frequencies trend for the unsymmetric cross-section beam.

<i>Step</i>	$-u_z/L$	<i>MODE</i>				
		1	2	3	4	5
		f_1	f_2	f_3	f_4	f_5
0	0.000	63.67	70.28	176.33	271.19	386.41
1	0.042	80.78	121.15	357.36	416.60	613.81
2	0.080	83.05	119.25	359.00	443.26	586.67
3	0.109	57.75	90.34	249.25	324.29	401.91
4	0.165	36.18	67.91	175.69	237.88	301.15
5	0.227	42.42	79.64	267.28	365.94	435.62
6	0.294	27.75	63.93	193.11	259.55	314.12
7	0.360	28.43	62.14	209.26	257.86	314.21
8	0.425	30.95	61.92	219.93	256.20	314.85
9	0.513	33.91	62.09	246.68	248.81	307.72
10	0.595	41.39	64.72	223.00	230.79	333.85
11	0.655	52.51	72.36	239.23	295.08	413.81
12	0.694	39.69	54.68	169.72	292.50	315.89
13	0.715	45.13	58.40	169.66	355.78	414.82
14	0.738	51.16	64.09	174.78	383.30	470.38
15	0.766	51.16	64.09	174.78	383.30	470.38
16	0.794	47.35	58.22	131.35	213.41	293.21
17	0.831	66.62	79.45	173.07	279.55	344.16

Table 4: Natural frequencies (Hz) values at most significant steps of the nonlinear analysis for first 5 modes.

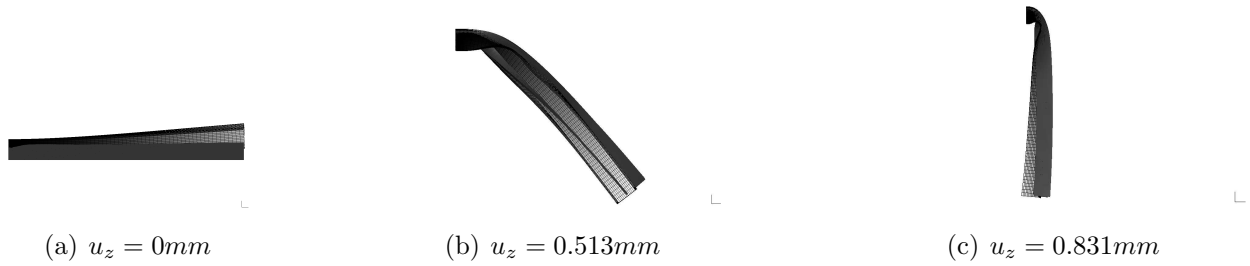


Figure 17: Modal shapes for first natural frequency, at load steps 0, 9 and 17.

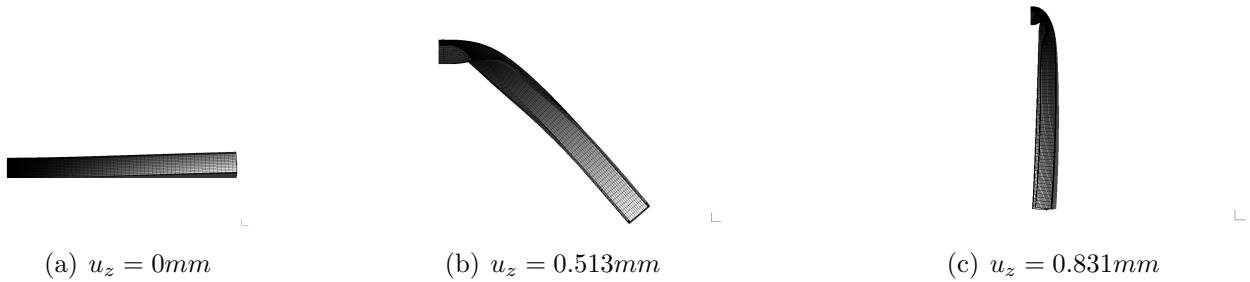


Figure 18: Modal shapes for second natural frequency, at load steps 0, 9 and 17.

(and subsequently of the associated natural frequencies) of the structure subjected to large deformations.

References

- [1] M.A. Biot. Non-linear theory of elasticity and the linearized case for a body under initial stress. *The London, Edinburgh, and Dublin Philosophical Magazine and Journal of Science*, 27(183):468–489, 1939.
- [2] G. Herrmann. The influence of initial stress on the dynamic behavior of elastic and viscoelastic plates. *Publ. Int. Assoc. Bridge Struct. Eng.*, 16:275–294, 1956.
- [3] R.W. Ogden and D.G. Roxburgh. The effect of pre-stress on the vibration and stability of elastic plates. *International Journal of Engineering Science*, 31(12):1611–1639, 1993.
- [4] H. Abramovich, D. Govich, and A. Grunwald. Buckling prediction of panels using the vibration correlation technique. *Progress in Aerospace Sciences*, 78:62–73, 2015.
- [5] H. Lurie. *Lateral vibrations as related to structural stability*. PhD thesis, California Institute of Technology, 1950.
- [6] A.W. Leissa. *Vibration of plates*. Technical report, OHIO STATE UNIV COLUMBUS, 1969.
- [7] A.W. Leissa. *Vibration of shells*, volume 288. Scientific and Technical Information Office, National Aeronautics and Space Administration Washington, 1973.
- [8] A.W. Leissa and M.S. Qatu. *Vibrations of Continuous Systems*. McGraw-Hill, 2011.

- [9] W.Y. Tseng and J. Dugundji. Nonlinear vibrations of a buckled beam under harmonic excitation. *Journal of applied mechanics*, 38(2):467–476, 1971.
- [10] N. Yamaki and A. Mori. Non-linear vibrations of a clamped beam with initial deflection and initial axial displacement, part i: Theory. *Journal of Sound and Vibration*, 71(3):333–346, 1980.
- [11] N. Yamaki, K. Otomo, and A. Mori. Non-linear vibrations of a clamped beam with initial deflection and initial axial displacement, part ii: Experiment. *Journal of Sound and Vibration*, 71(3):347–360, 1980.
- [12] G.R. Bhashyam and G. Prathap. Galerkin finite element method for non-linear beam vibrations. *Journal of Sound and Vibration*, 72(2):191–203, 1980.
- [13] W. Lacarbonara, A.H. Nayfeh, and W. Kreider. Experimental validation of reduction methods for nonlinear vibrations of distributed-parameter systems: analysis of a buckled beam. *Nonlinear Dynamics*, 17(2):95–117, 1998.
- [14] A. Fallah and M.M. Aghdam. Nonlinear free vibration and post-buckling analysis of functionally graded beams on nonlinear elastic foundation. *European Journal of Mechanics-A/Solids*, 30(4):571–583, 2011.
- [15] H. Asadi and M.M. Aghdam. Large amplitude vibration and post-buckling analysis of variable cross-section composite beams on nonlinear elastic foundation. *International Journal of Mechanical Sciences*, 79:47–55, 2014.
- [16] E. Carrera, G. Giunta, and M. Petrolo. *Beam Structures: Classical and Advanced Theories*. John Wiley & Sons, 2011.
- [17] E. Carrera, M. Cinefra, M. Petrolo, and E. Zappino. *Finite Element Analysis of Structures through Unified Formulation*. John Wiley & Sons, Chichester, West Sussex, UK., 2014.
- [18] E. Carrera, M. Maiarú, and M. Petrolo. Component-wise analysis of laminated anisotropic composites. *International Journal of Solids and Structures*, 49(13):1839–1851, 2012.
- [19] M. Filippi and E. Carrera. Capabilities of 1d cuf-based models to analyze metallic/composite rotors. In *8th Australasian Congress on Applied Mechanics: ACAM 8*, page 315. Engineers Australia, 2014.
- [20] E. Carrera and A. Pagani. Free vibration analysis of civil engineering structures by component-wise models. *Journal of Sound and Vibration*, 333(19):4597–4620, 2014.
- [21] E. Carrera, M. Petrolo, and A. Varello. Advanced beam formulations for free-vibration analysis of conventional and joined wings. *Journal of Aerospace Engineering*, 25(2):282–293, 2011.
- [22] A. Pagani, M. Petrolo, G. Colonna, and E. Carrera. Dynamic response of aerospace structures by means of refined beam theories. *Aerospace Science and Technology*, 46:360–373, 2015.

- [23] F. Miglioretti and E. Carrera. Application of a refined multi-field beam model for the analysis of complex configurations. *Mechanics of Advanced Materials and Structures*, 22(1-2):52–66, 2015.
- [24] A. Pagani and E. Carrera. Unified formulation of geometrically nonlinear refined beam theories. *Mechanics of Advanced Materials and Structures*, 2016. In Press.
- [25] A. Pagani and E. Carrera. Large-deflection and post-buckling analyses of laminated composite beams by carrera unified formulation. *Composite Structures*, 170:40–52, 2017.
- [26] E. Carrera and M. Petrolo. Refined beam elements with only displacement variables and plate/shell capabilities. *Meccanica*, 47(3):537–556, 2012.
- [27] K.J. Bathe. *Finite element procedure*. Prentice hall, Upper Saddle River, New Jersey, USA, 1996.
- [28] K.E. Bisshopp and D.C. Drucker. Large deflection of cantilever beams. *Quarterly of Applied Mathematics*, 3(3):272–275, 1945.